Citation:
Jeffrey D. Udall and Fow-Sen Choa "Comparing energy levels in brain regions of interest in ADHD subjects", Proc. SPIE 12123, Smart Biomedical and Physiological Sensor Technology XIX, 1212305 (8 June 2022); https://doi.org/10.1117/12.2618207

DOI:
https://doi.org/10.1117/12.2618207

Comparing energy levels in brain regions of interest in ADHD subjects

Jeffrey Udall, Fow-Sen Choa

Jeffrey D. Udall, Fow-Sen Choa, "Comparing energy levels in brain regions of interest in ADHD subjects," Proc. SPIE 12123, Smart Biomedical and Physiological Sensor Technology XIX, 1212305 (8 June 2022); doi: 10.1117/12.2618207

Event: SPIE Defense + Commercial Sensing, 2022, Orlando, Florida, United States

Comparing energy levels in brain regions of interest in ADHD subjects

Jeffrey D. Udall, Fow-Sen Choa
University of Maryland Baltimore County, Computer Science and Electrical Engineering Department, 1000 Hilltop Circle, ITE 325, Baltimore, Maryland 21250

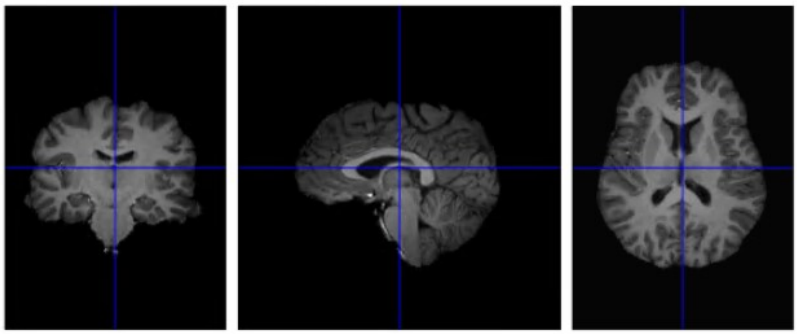

Figure 1. Anatomical MRI image from the NewYork_a_ADHD data set. (2022 The International Neuroimaging Data-sharing Initiative (INDI) www.nitrc.org)

ABSTRACT

Energy Landscape analysis is a statistical method of examining networks in the brain. In this study we apply this technique to analyze and compare resting state fMRI brain scan data from brain Regions of Interest (ROIs) in subjects with Attention Deficit Hyperactivity Disorder (ADHD) to the same ROI activity in a control group of similar genders and ages. 192 temporal data samples were extracted from the fMRI data and using masks 90 spatial AAL ROIs were isolated for each of the fifty subjects. These (90 x 50) ROI time data files were then combined into one file per subject, and then concatenated into two groups: ADHD and Control. The two concatenated files were then normalized, binarized, and processed with the Energy Landscape Analysis Toolbox (ELAT) by Takahiro Ezaki. The ELAT analysis produced Activation Maps, Disconnectivity Graphs, and Local Minima figures showing the comparative energy levels of the ROIs grouped into nine separate sub-networks.

These results were then compared between groups to obtain candidate biomarkers that could be used to distinguish the ADHD subjects from the Control group. Our results point to significant differences in the energy levels of brain states between the two groups in the Salience (SAL), Frontoparietal (FPN), and Attention (ATN) sub-networks. These areas of the brain are associated with language, self-awareness, spatial attention, emotions, and social behavior.

Keywords: fMRI, energy landscape analysis, brain networks, ROI networks, ADHD, activation maps, disconnectivity graphs

INTRODUCTION

Regions of interest (ROI) in the human brain have identified to help analyze and compare different brains using a common reference. In this project we analyze resting state fMRI data sets from subjects who belong to two comparable groups of similar age and gender, an Attention Deficit Hyperactivity Disorder (ADHD) subject group and a Control group. We then compare the ROI networks in the data sets to look for markers that could be used to differentiate subjects with the identified disorder, in this case ADHD. We then examine possible reasons for these differences based on longstanding research into the functions of the ROI and their sub-networks.

This comparison will be made primarily by Energy Landscape analysis [1], a statistical analysis technique used to compare the fMRI time series data sets and construct an “energy landscape” of binarized signals in brain ROIs obtained

Smart Biomedical and Physiological Sensor Technology XIV, edited by Brian M. Cullum, Douglas Kiehl, Eric S. McLamore,
Proc. of SPIE Vol. 12123, 1212305 · © 2022 SPIE · 0277-786X · doi: 10.1117/12.2618207

from fMRI time series data. This data is then presented using Activation Maps of ROI states, Disconnectivity Graphs of energy levels, and Local Minima plots. Our goal in examining fMRI data from ADHD subjects (see Figure 2) is an attempt to find biological markers in the brain activity processed by energy landscape to isolate significant differences in brain activity that can be generalized to the ADHD disorder and may eventually be used in a diagnostic manner by technicians and medical professionals examining patient's resting state fMRI data.

The symptoms of ADHD give us a clue of what resting state brain networks to examine. According to the Mayo Clinic, "Adult attention-deficit/hyperactivity disorder is a mental health disorder that includes a combination of persistent problems, such as difficulty paying attention, hyperactivity, and impulsive behavior. Adult ADHD can lead to unstable relationships, poor work or school performance, low self-esteem, and other problems [3]."

Currently a diagnosis of ADHD can be very time consuming and intensive. It involves many tests, taken over many hours, or even several days, and can involve neuroanalysis by several psychologists and psychiatrists before a confident diagnosis can be made. By examining resting state networks via energy landscape analysis which include areas of the brain involved in attention, hyper-activity, and impulsiveness we hope to identify promising biomarker brain states for ADHD. It is anticipated that fMRI biomarkers can be used in the future to provide quick, easy, and affordable diagnosis techniques for people suffering with ADHD.

NewYork_a_ADHD(age order)				NewYork_a(age order)			
sub23844	12	f	20.69	sub07578	5	f	20.69
sub08595	2	m	23.38	sub16607	11	m	21
sub22608	11	f	23.43	sub28808	20	f	23.34
sub31554	14	f	24.39	sub30247	24	f	24.03
sub14299	4	f	24.58	sub41546	33	f	24.03
sub77903	24	m	24.66	sub66085	57	m	24.15
sub73035	22	m	26	sub83978	68	m	25.63
sub22349	10	m	26.15	sub44515	35	m	25.71
sub20691	9	m	26.35	sub47087	39	m	25.72
sub53461	16	m	27	sub63280	55	m	25.79
sub15758	6	m	32.84	sub83782	67	m	25.98
sub59796	19	m	34.65	sub80566	63	m	26.33
sub03951	1	m	37.32	sub95971	79	m	27.24
sub48803	15	m	37.98	sub29216	21	m	29.06
sub84371	25	m	38.26	sub21212	16	m	30.83
sub77203	23	m	40.23	sub01912	1	m	31.53
sub69779	21	m	40.75	sub54696	47	m	32.16
sub12486	3	m	40.77	sub17078	12	m	34.19
sub54828	17	m	41.34	sub82228	64	m	35
sub63915	20	m	44.91	sub45217	37	m	40.48
sub24528	13	m	45.9	sub58451	51	m	41.71
sub17109	7	m	46.15	sub19579	14	m	46.59
sub14465	5	m	47.06	sub10582	8	m	47.98
sub20676	8	m	49.19	sub33581	29	m	49.03
sub56734	18	f	50.9	sub91953	74	f	49.16

Figure 2. Subject lists using the NewYork_a_ADHD and NewYork_a (control) groups from the FCP Classic Data Sharing Samples of the 1000 Functional Connectomes Project [4] - The International Neuroimaging Data-sharing Initiative (INDI) www.nitrc.org (2022)

2. FMRI DATA

The data used in this study was resting state fMRI data obtained from NITRC's FCP Classic Data Sharing Samples website [4]. The fMRI data files were formatted as NIFTI files containing 39 slices and 192 time point samples each. They also included anatomical MRI images (Figure 1) which were not directly used in this study. The patient data is from the group named *NewYork_a_ADHD* and consisted of twenty-five participants (20M/5F) ages 20-50. The control group was obtained from a similar data set from the same fMRI machine, *NewYork_a*. The subject list from NewYork_a was narrowed down from 84 to 25 subjects to obtain a more direct comparison using similar genders (20M/5F) and age ranges (20-50). (See Figure 2.)

ROIs in the AAL atlas					
Index	Regions	Network		Additional	
1, 2	Precental gyrus	Sensorimotor	SSM		
3, 4	Superior frontal gyrus, dorsolateral	Frontoparietal	FPN		
5, 6	Superior frontal gyrus, orbital part	Frontoparietal	FPN		
7, 8	Middle frontal gyrus	Frontoparietal	FPN	Attention	Salience
9, 10	Middle frontal gyrus, orbital part	Frontoparietal	FPN		
11, 12	Inferior frontal gyrus, opercular part	Cingulo-opercular	CON		
13, 14	Inferior frontal gyrus, triangular part	Frontoparietal	FPN	Attention	Salience
15, 16	Inferior frontal gyrus, orbital part	None	NA		
17, 18	Rolandic operculum	Cingulo-opercular	CON	Audtory	
19, 20	Supplementary motor area	Sensorimotor	SSM		
21, 22	Olfactory cortex	None	NA		
23, 24	Superior frontal gyrus, medial	Default-mode	DMN		
25, 26	Superior frontal gyrus, medial orbital	Default-mode	DMN		
27, 28	Gyrus rectus	None	NA		
29, 30	Insula	Cingulo-opercular	CON	Salience	
31, 32	Anterior cingulate and paracingulate gyri	Default-mode	DMN	Salience	
33, 34	Median cingulate and paracingulate gyri	Cingulo-opercular	CON	Salience	
35, 36	Posterior cingulate gyrus	Default-mode	DMN		
37, 38	Hippocampus	None	NA		
39, 40	Parahippocampal gyrus	Default-mode	DMN		
41, 42	Amygdala	None	NA		
43, 44	Calcarine fissure and surrounding cortex	Visual	VIS		
45, 46	Cuneus	Visual	VIS		
47, 48	Lingual gyrus	Visual	VIS		
49, 50	Superior occipital gyrus	Visual	VIS		
51, 52	Middle occipital gyrus	Visual	VIS		
53, 54	Inferior occipital gyrus	Visual	VIS		
55, 56	Fusiform gyrus	Visual	VIS		
57, 58	Postcentral gyrus	Sensorimotor	SSM		
59, 60	Superior parietal gyrus	Attention	ATN	Salience	
61, 62	Inferior parietal, but supramarginal and angular gyri	Frontoparietal	FPN	Attention	
63, 64	Supramarginal gyrus	Cingulo-opercular	CON	Audtory	
65, 66	Angular gyrus	Default-mode	DMN		
67, 68	Precuneus	Default-mode	DMN		
69, 70	Paracentral lobule	Sensorimotor	SSM		
71, 72	Caudate nucleus	Subcortical	SUB		
73, 74	Lenticular nucleus, putamen	Subcortical	SUB		
75, 76	Lenticular nucleus, pallidum	Subcortical	SUB		
77, 78	Thalamus	Subcortical	SUB		
79, 80	Heschl gyrus	Audtory			
81, 82	Superior temporal gyrus	Attention	ATN	Audtory	
83, 84	Temporal pole: superior temporal gyrus	Cingulo-opercular	CON		
85, 86	Middle temporal gyrus	Default-mode	DMN		
87, 88	Temporal pole: middle temporal gyrus	Default-mode	DMN		
89, 90	Inferior temporal gyrus	None	NA		

7, 8	Middle frontal gyrus	Attention	ATN
13, 14	Inferior frontal gyrus, triangular part	Attention	ATN
59, 60	Superior parietal gyrus	Attention	ATN
61, 62	Inferior parietal, but supramarginal and angular gyri	Attention	ATN
81, 82	Superior temporal gyrus	Attention	ATN
17, 18	Rolandic operculum	Audtory	AUD
63, 64	Supramarginal gyrus	Audtory	AUD
79, 80	Heschl gyrus	Audtory	AUD
83, 84	Temporal pole: superior temporal gyrus	Audtory	AUD
11, 12	Inferior frontal gyrus, opercular part	Cingulo-opercular	CON
17, 18	Rolandic operculum	Cingulo-opercular	CON
29, 30	Insula	Cingulo-opercular	CON
33, 34	Median cingulate and paracingulate gyri	Cingulo-opercular	CON
63, 64	Supramarginal gyrus	Cingulo-opercular	CON
83, 84	Temporal pole: superior temporal gyrus	Cingulo-opercular	CON
23, 24	Superior frontal gyrus, medial	Default-mode	DMN
25, 26	Superior frontal gyrus, medial orbital	Default-mode	DMN
31, 32	Anterior cingulate and paracingulate gyri	Default-mode	DMN
35, 36	Posterior cingulate gyrus	Default-mode	DMN
39, 40	Parahippocampal gyrus	Default-mode	DMN
65, 66	Angular gyrus	Default-mode	DMN
67, 68	Precuneus	Default-mode	DMN
85, 86	Middle temporal gyrus	Default-mode	DMN
87, 88	Temporal pole: middle temporal gyrus	Default-mode	DMN
3, 4	Superior frontal gyrus, dorsolateral	Frontoparietal	FPN
5, 6	Superior frontal gyrus, orbital part	Frontoparietal	FPN
7, 8	Middle frontal gyrus	Frontoparietal	FPN
9, 10	Middle frontal gyrus, orbital part	Frontoparietal	FPN
13, 14	Inferior frontal gyrus, triangular part	Frontoparietal	FPN
61, 62	Inferior parietal, but supramarginal and angular gyri	Frontoparietal	FPN
7, 8	Middle frontal gyrus	Salience	SAL
13, 14	Inferior frontal gyrus, triangular part	Salience	SAL
29, 30	Insula	Salience	SAL
31, 32	Anterior cingulate and paracingulate gyri	Salience	SAL
33, 34	Median cingulate and paracingulate gyri	Salience	SAL
59, 60	Superior parietal gyrus	Salience	SAL
1, 2	Precental gyrus	Sensorimotor	SSM
19, 20	Supplementary motor area	Sensorimotor	SSM
57, 58	Postcentral gyrus	Sensorimotor	SSM
69, 70	Paracentral lobule	Sensorimotor	SSM
71, 72	Caudate nucleus	Subcortical	SUB
73, 74	Lenticular nucleus, putamen	Subcortical	SUB
75, 76	Lenticular nucleus, pallidum	Subcortical	SUB
77, 78	Thalamus	Subcortical	SUB
43, 44	Calcarine fissure and surrounding cortex	Visual	VIS
45, 46	Cuneus	Visual	VIS
47, 48	Lingual gyrus	Visual	VIS
49, 50	Superior occipital gyrus	Visual	VIS
51, 52	Middle occipital gyrus	Visual	VIS
53, 54	Inferior occipital gyrus	Visual	VIS
55, 56	Fusiform gyrus	Visual	VIS

Figure 3. AAL Regions of Interest in the brain with their subnetwork affiliations

3. DATA PROCESSING

Processing the fMRI data took several steps. The first task was to extract the time series date from each subject. Much of the pre-processing of the NIFTI files, such as pre-processing data for removing noise and enhancing the signal, was assumed to have already been performed and this study proceeded accordingly with ROI analysis and formatting the data for the Energy Landscape Analysis Toolbox (ELAT) MATLAB program by Ezaki [1].

The data extraction began by running the Statistical Parametric Mapping (SPM) program in MATLAB. This was used to import the NIFTI fMRI files into MATLAB (see Figure 4). Next, another MATLAB program, Response Exploration (REX), was used to extract the time series signal data. REX applied a mask to each fMRI file to divide the extracted data into 90 anatomical ROIs (see Figure 3). The output from REX was a MATLAB data structure containing 90 rows and 192 columns with the measured state of each ROI at each time sample. This data was then concatenated into two large files for each group, ADHD and Control, containing 4800 time samples each (25x192). These two concatenated files provided an extended time series data set for the Energy Landscape program to apply its statistical analysis algorithm.

The two ROI data files, ADHD and Control, were then further divided into functional resting state networks (see Figure 4, right side) in preparation for energy landscape analysis. Some networks, such as the Default-Mode network (DMN) and Visual network (VIS), contain many ROIs—18 and 14 ROIs respectfully. This is too many regions for the Energy Landscape Analysis Tool (ELAT) to process at once in one file, so these two networks were divided into two sub-networks each (Left and Right). The resulting 11 ROI network files from the ADHD and Control groups were then analyzed using energy landscape analysis.

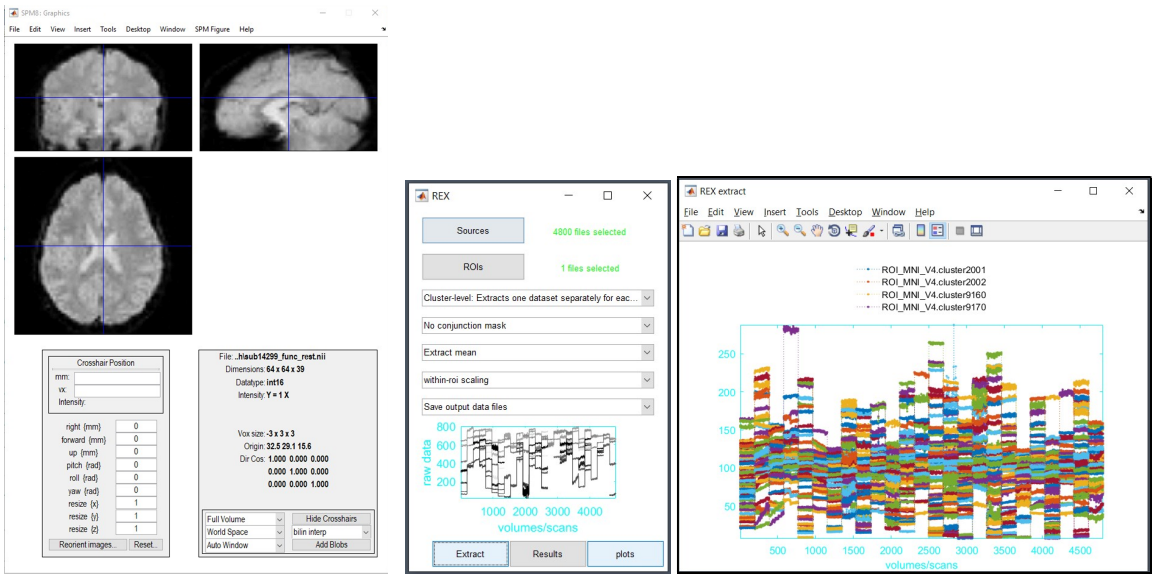

Figure 4. fMRI file open in the Statistical Parametric Mapping (SPM) program (left). fMRI file in REX used to extract 192 time data samples into AAL90 ROIs using applied masks (center and right).

4. ENERGY LANDSCAPE ANALYSIS

After the data was formatted, concatenated, and parsed into ROI networks it was brought into MTLAB and processed by the Energy Landscape Analysis Tool [1]. The ELAT binarized the data and performed pairwise maximum entropy statistical analysis [1] to produce a "energy landscape" relationship between the activation states of the ROIs in the resting state networks. The ELAT output Activation Maps, Disconnectivity Graphs, and Local Minima Basin figures for each ROI network (see Figure 5).

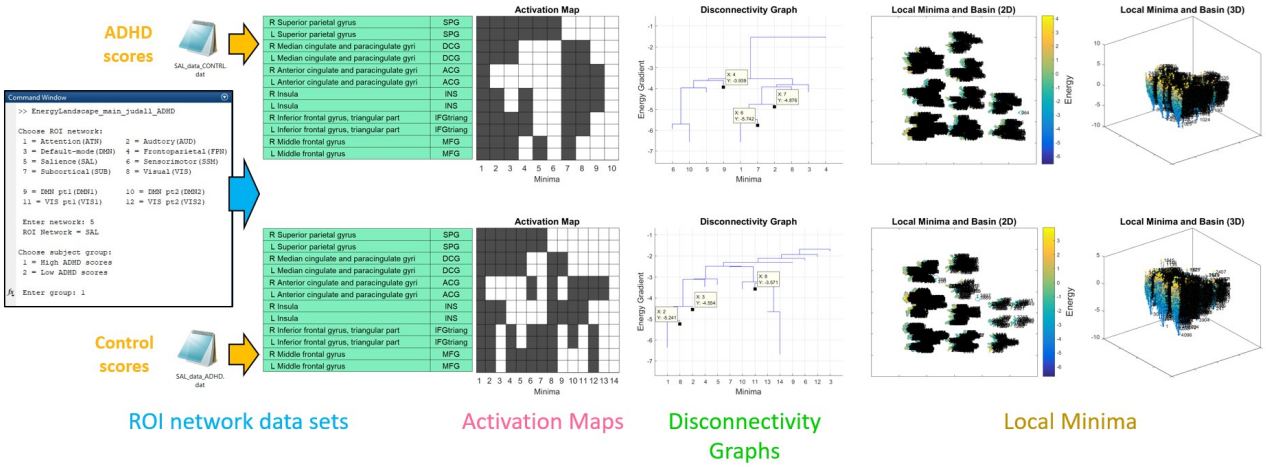

Figure 5. Energy Landscape analysis output. Each ROI network was processed to produce an Activation Map, Disconnectivity Graph, and Local Minima Basin figures for each group (in this case High ADHD and Low ADHD).

The Activation Maps are grids with each box representing the activation state of a particular ROI. White, or 1, indicates activation and black, or 0. Each column of the Activation Map represents the combined state of the ROIs in the network. The Disconnectivity graphs represent how each state is relates to other states in energy space. States in the graph are separated, or disconnected, from each other in the energy landscape, with the lower energy levels representing the increasing frequency the state is occupied during the sample times. The further apart two states are, the more unlikely

they are to transition between the two states. The Local Minima figures energy landscape can be represented as a minima (valleys) and maxima (hills) along a 2D or 3D surface represented in in.

The relationship between the energy levels in states of activation/deactivation of ROI networks is the heart of energy landscape analysis and can help compare the brain states of two separate groups, like the ADHD and Control groups. By examining the differences between the populations, and searching for a state of activity in ROI of the brain that may indicate a disorder or disease in the brain. The difference in energy levels between two groups for the same brain ROI energy state can then be used as a potential biomarker to identify the disorder more quickly in the future.

This study of the ADHD resting state fMRI data focused on four ROI networks (Salience, Frontoparietal, Attention, and Default-Mode). These were chosen for the initial indications of possible biomarker ROI states. (For the full ADHD VS Control group Energy Landscape analysis data see Appendix.)

4.1 Salience (SAL) network

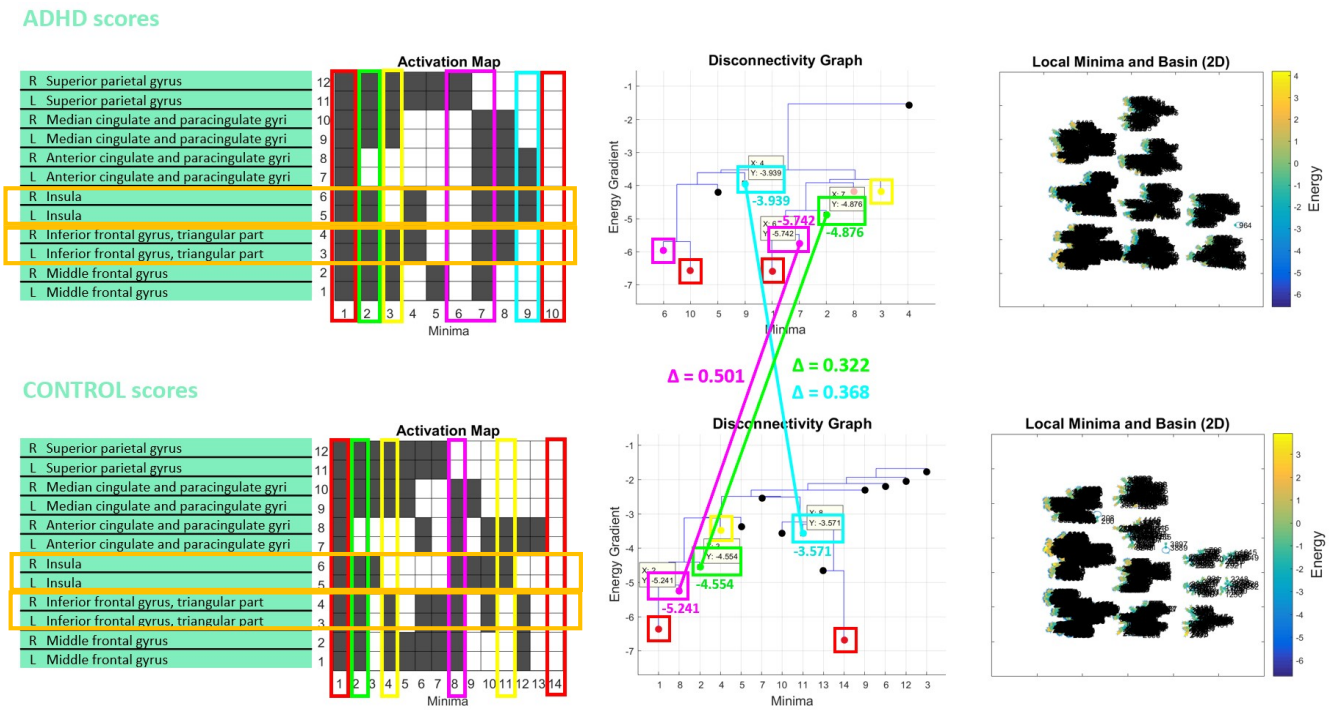

Figure 6. Salience Network Energy Landscape output

The Salience (SAL) network helps the brain detect noticeable qualities (salience). It includes the brain areas of the insula and triangular gyrus. The insula (Figure 6 and 7, ROIs 6 and 5) has important connections to language and visual-vestibular integration. The triangular gyrus (Figure 6 and 7, ROIs 3 and 4), also known as Brodmann's area 45, it is one of two regions that make up Broca's area together with Brodmann's area 44 (a.k.a. Pars Opercularis).

Broca's area is well known to be involved in expressive aspects of spoken and written language. More specifically, the pars triangularis is involved with semantic processing of language. In the non-dominant hemisphere, the same cortical region is involved in non-verbal communication such as gesticulation, facial expression and modulation of timing and intonation of speech.

In the examination of SAL eight ROI states of interest were identified (see Figure 7), with four of them being strong candidates: 753, 760, 1280, and 4084. These states had very low energy minima, representing a high frequency of occurrence in the resting state fMRI data. SAL State 760 also registered a large delta between the ADHD and Control groups, representing a large difference in the frequency of the state between groups. Performing two-tailed t-tests in MATLAB on these states produce p-values of < 0.02, indicating that these difference between groups are statistically significant (see box plots in Figure 8).

	SAL States with low p-values								
12	R Superior parietal gyrus	0	0	0	0	0	1	1	1
11	L Superior parietal gyrus	0	0	0	0	1	1	1	1
10	R Median cingulate and paracingulate gyri	1	1	1	1	0	1	1	1
9	L Median cingulate and paracingulate gyri	0	0	0	1	0	1	1	1
8	R Anterior cingulate and paracingulate gyri	1	1	1	1	1	0	1	1
7	L Anterior cingulate and paracingulate gyri	1	1	1	1	1	1	1	1
6	R Insula	1	1	1	0	1	1	0	1
5	L Insula	1	1	1	1	1	1	1	1
4	R Inferior frontal gyrus, triangular part	0	0	0	0	1	0	0	0
3	L Inferior frontal gyrus, triangular part	0	1	1	0	1	0	0	0
2	R Middle frontal gyrus	0	0	1	0	1	1	1	1
1	L Middle frontal gyrus	0	1	1	0	1	1	1	1
	States	753	758	760	977	1280	3956	4052	4084
	ADHD Min En	-3.47	-2.61	-3.1	-2.61	-3.69	-1.22	-1.55	-3.22
	CONTRL Min En	-1.74	-0.84	-0.78	-1.17	-2.04	-2.59	-2.59	-3.93
	Δ Min Energy	1.731	1.766	2.329	1.445	1.649	1.37	1.038	0.718
	p-value	0.0063	0.0142	0.0098	0.0161	0.015	0.0027	0.0106	0.0199

Figure 7. Most promising states for potential biomarkers in the SAL network after further investigation. These states had promising results from t-tests (see box plots) as well as low energy values.

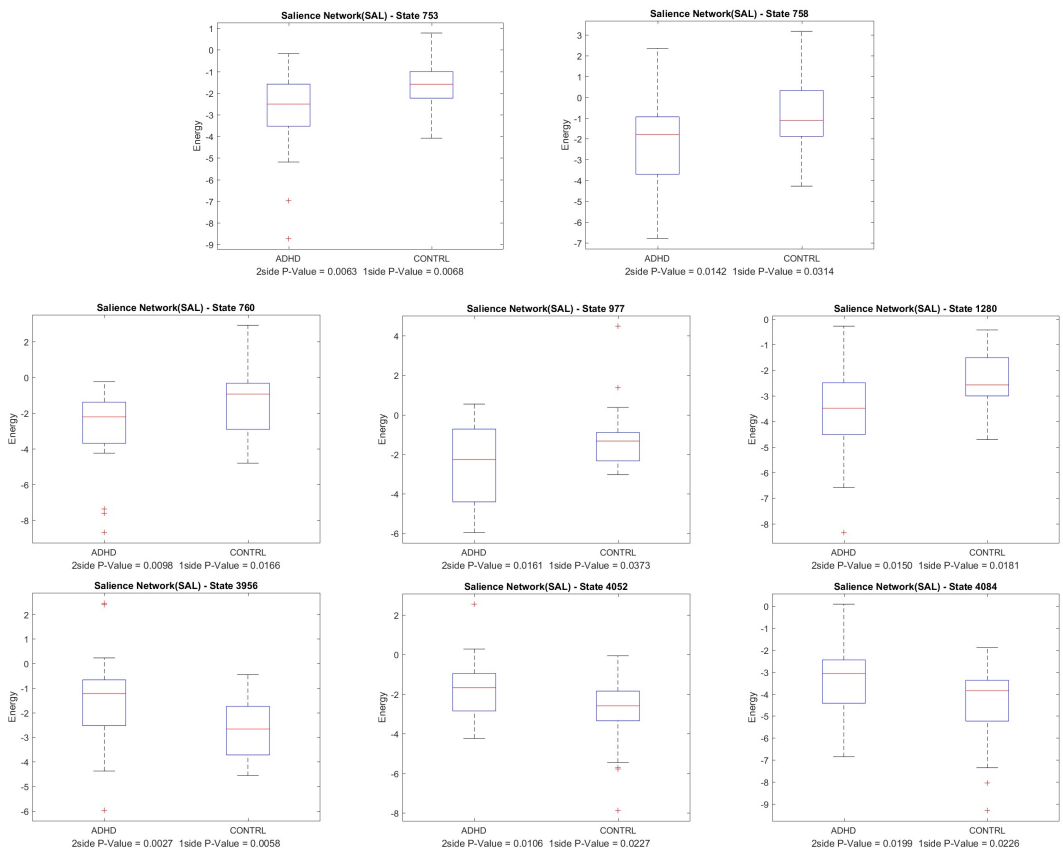

Figure 8. Box plots illustrating the t-test results of the most promising states for potential biomarkers in the SAL network.

While these states appear to have potential as fMRI biomarkers for ADHD diagnosis, further analysis is needed to fully examine if the activation patterns of these states, and their constituent ROIs, would be useful and accurate in practical real-world testing.

4.2 Frontoparietal network (FPN)

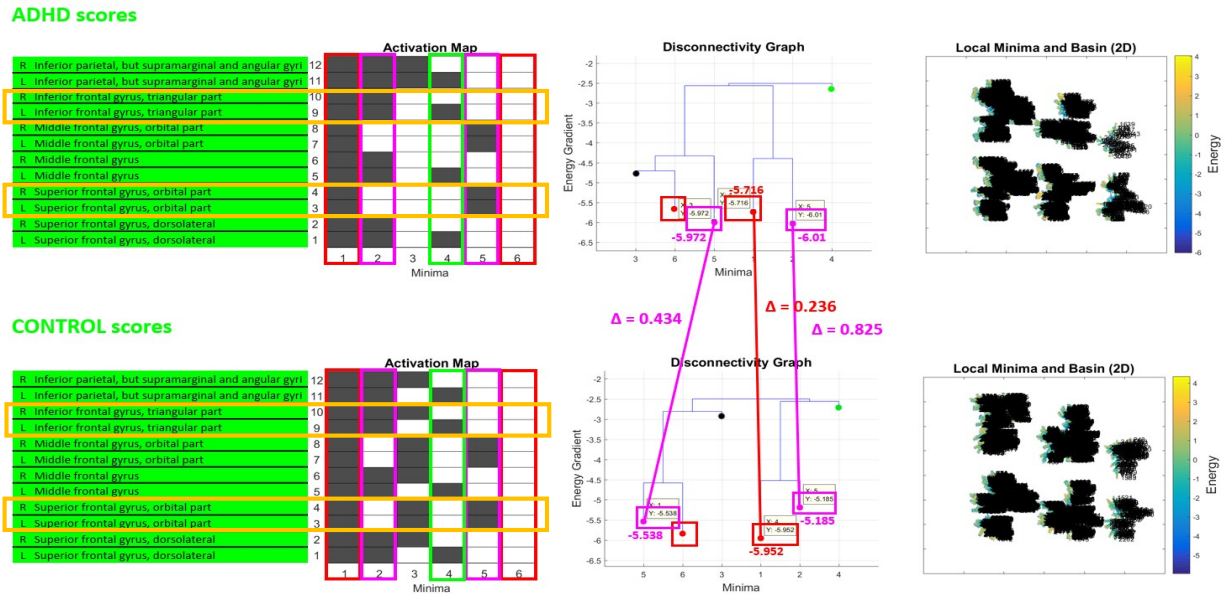

Figure 9. Frontoparietal Network Energy Landscape output

In the Frontoparietal network (FPN), is involved with memory and attention in the brain. As with the SAL network, in includes the triangular gyrus (Figure 9 and 10, ROIs 10 and 9), involved with semantic processing of language, and superior frontal gyrus (Figure 9 and 10, ROIs 4 and 3) involved in self-awareness.

	FPN States with low p-values			
12	Inferior parietal, but supramarginal and angular gyri	1	1	1
11	Inferior parietal, but supramarginal and angular gyri	0	1	1
10	Inferior frontal gyrus, triangular part	0	1	1
9	Inferior frontal gyrus, triangular part	0	0	1
8	Middle frontal gyrus, orbital part	1	1	1
7	Middle frontal gyrus, orbital part	1	0	0
6	Middle frontal gyrus	0	1	1
5	Middle frontal gyrus	0	1	1
4	Superior frontal gyrus, orbital part	1	0	0
3	Superior frontal gyrus, orbital part	1	1	1
2	Superior frontal gyrus, dorsolateral	1	1	1
1	Superior frontal gyrus, dorsolateral	0	1	1
	States	2255	3768	4024
	ADHD Min En	-2.89	-2.63	-3.78
	CONTRL Min En	-1.64	-1.34	-2.71
	Δ Min Energy	1.245	1.285	1.072
	p-value	0.0115	0.0022	0.0145

Figure 10. Most promising states for potential biomarkers in the FPN after further investigation. These states had promising results from t-tests (see box plots) as well as low energy values.

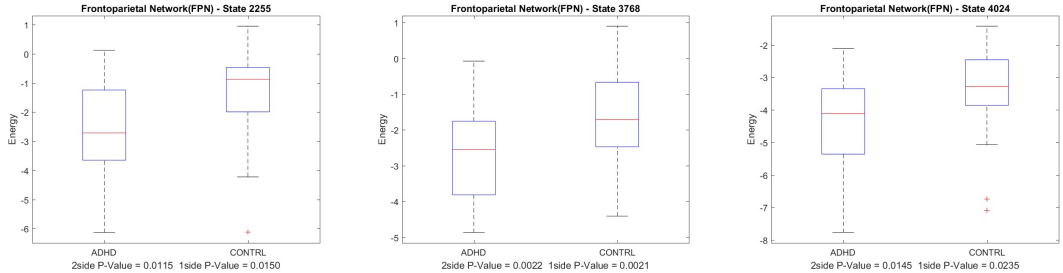

Figure 11. Box plots illustrating the t-test results of the most promising states for potential biomarkers in the FPN.

Results of the energy landscape analysis of FPN indicate three states may represent possible biomarkers, with FPN State 4024 having significantly low energy minima in both ADHD and Control groups (see Figure 10). The t-test p-value results indicate that all three states represent statistically significant differences in the two groups (see box plots in Figure 11).

4.3 Attention network (ATN)

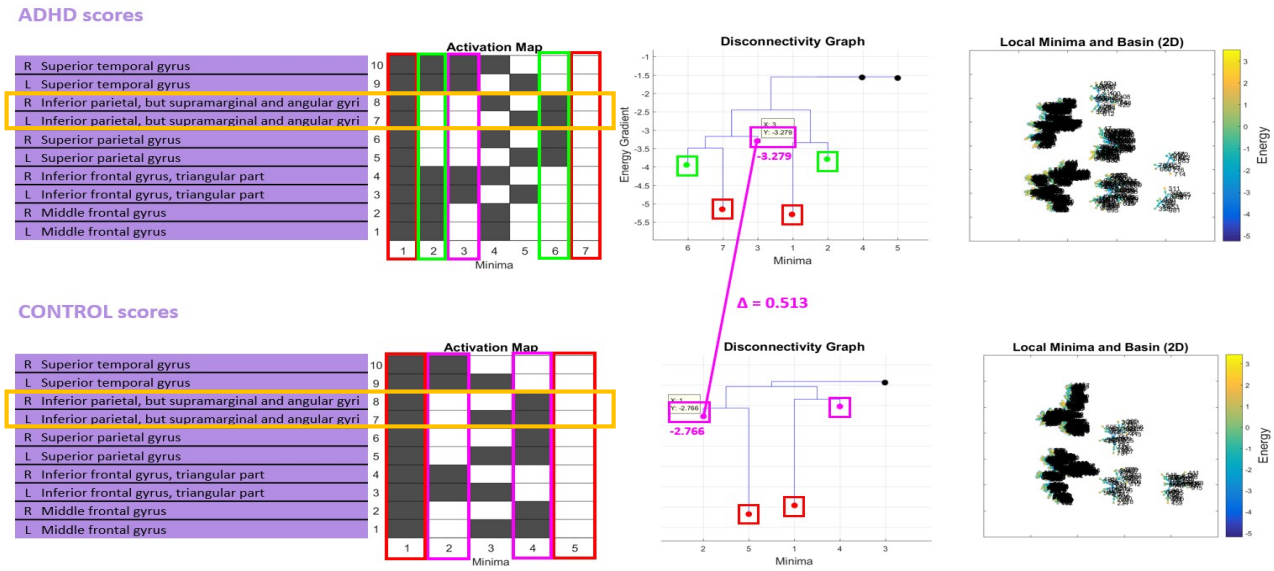

Figure 12. Attention Network Energy Landscape output

The Attention network (ATN) involved in spatial, visual, and auditory attention. The ATN contains the inferior parietal and superior parietal gyrus in this ROI network. The inferior parietal (Figure 12, ROIs 8 and 7) is involved with sensorimotor integration, spatial attention and visuomotor and auditory processing. The ATN contains a possible biomarker ROI state for ADHD, in ATN State 641 (see Figure 13).

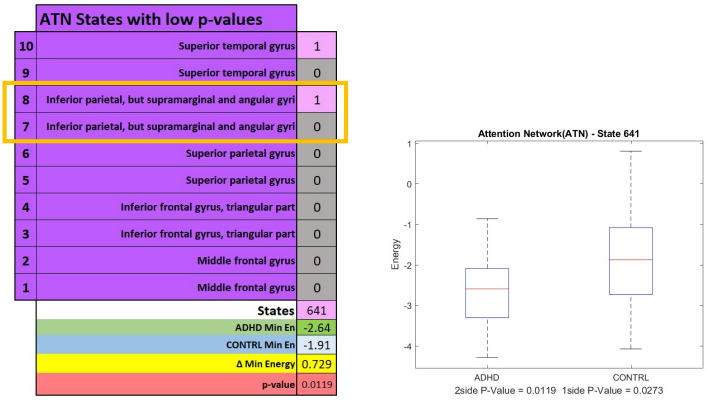

ATN States with low p-values		
10	Superior temporal gyrus	1
9	Superior temporal gyrus	0
8	Inferior parietal, but supramarginal and angular gyri	1
7	Inferior parietal, but supramarginal and angular gyri	0
6	Superior parietal gyrus	0
5	Superior parietal gyrus	0
4	Inferior frontal gyrus, triangular part	0
3	Inferior frontal gyrus, triangular part	0
2	Middle frontal gyrus	0
1	Middle frontal gyrus	0
	States	641
	ADHD Min En	-2.64
	CONTRL Min En	-1.91
	Δ Min Energy	0.729
	p-value	0.0119

Figure 13. Most promising states for potential biomarkers in the ATN after further investigation. This state had a promising result from the t-test (see box plot) as well as low energy values (left). Box plot illustrating the t-test results of the most promising state for potential biomarkers in the ATN (right).

The energy minima of ATN State 641 (-2.64) does not have as high of a significance as other potential biomarkers in other networks. This is a surprising result given that the disorder examined in this study is Attention Deficit Hyperactivity Disorder. It is possible that further studies may find better biomarker candidates in this network, but the results of this study point to a remarkable lack of indicators in ATN.

4.4 Default-Mode network (DMN)

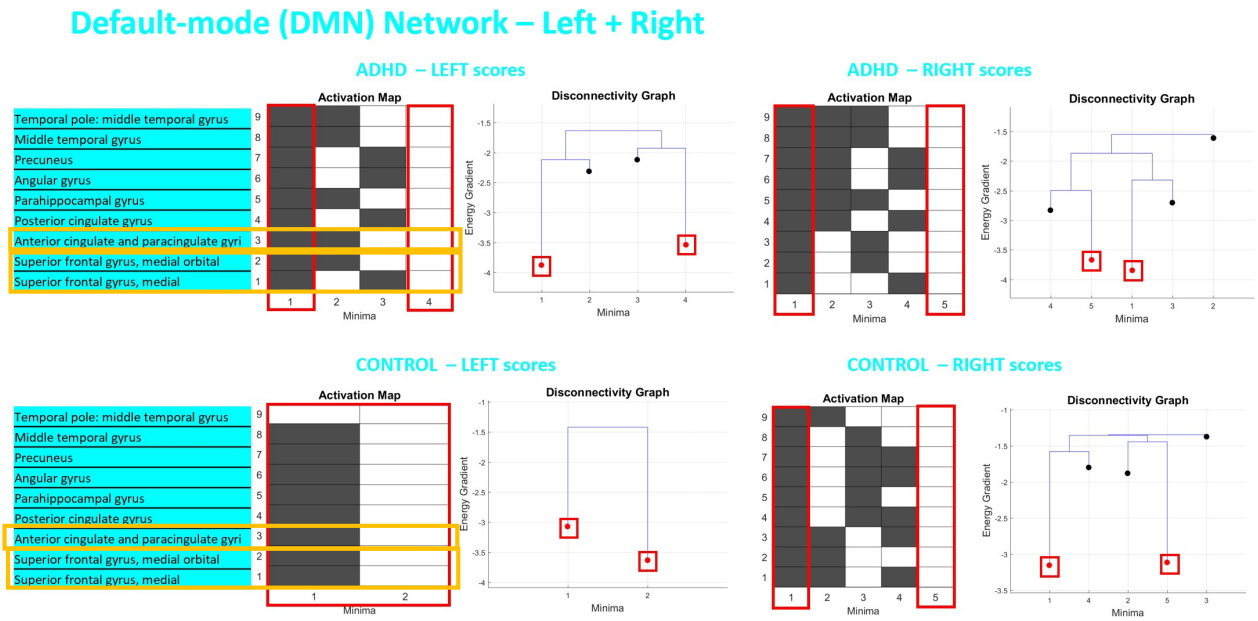

Figure 14. Default-Mode Network Energy Landscape output (left-side)

The Default-Mode network (DMN) serves as a kind of default brain state when transitioning from other networks. The DMN contains the Superior frontal gyrus (Figure 14, ROIs 1 and 2) is involved in self-awareness, in coordination with the action of the sensory system. The anterior part of the cingulate (Figure 14, ROI 3) is involved in certain higher-level functions, such as attention allocation, reward anticipation, decision-making, ethics and morality, impulse control (e.g., performance monitoring and error detection), and emotion.

Due to the large size of the DMN, it was necessary to split it into two separate networks, Left and Right, in order to process it using the Energy Landscape program. This may have comprised the effectiveness of the energy analysis, but the initial results were promising with large deltas in the energy minima between groups in DMN-R State 1 and 512, of 0.682 and 0.553 respectively (see Figure 15).

ROIs		DMNR - ADHD				
9	Temporal pole: middle temporal gyrus	0	0	0	1	1
8	Middle temporal gyrus	0	0	0	1	1
7	Precuneus	0	0	1	0	1
6	Angular gyrus	0	0	1	0	1
5	Parahippocampal gyrus	0	0	0	1	1
4	Posterior cingulate gyrus	0	0	1	0	1
3	Anterior cingulate and paracingulate gyri	0	1	0	1	1
2	Superior frontal gyrus, medial orbital	0	1	0	1	1
1	Superior frontal gyrus, medial	0	1	1	0	1
	States	1	8	106	407	512
	Min Energy	-3.850	-1.615	-2.702	-2.821	-3.685
	p-value	0.031	0.334	0.018	0.032	0.154

ROIs	DMNR - CONTRL				
9	0	0	1	1	1
8	0	1	0	1	1
7	0	1	0	0	1
6	0	1	0	0	1
5	0	1	0	1	1
4	0	1	0	0	1
3	0	0	1	0	1
2	0	0	1	1	1
1	0	0	1	0	1
States	1	249	264	403	512
Min Energy	-3.168	-1.878	-1.380	-1.797	-3.132
p-value	0.031	0.22	0.44	0.292	0.154

Figure 15. Default-Mode Network Energy Landscape output (right-side) P-values from the t-test indicate the differences between groups are not significant.

Perhaps because of the splitting into two groups, the t-test p-values of DMN-R State 1 and 512 were both too high to represent significant differences between the groups (0.031 and 0.154 respectively). (See Figure 15.)

The other ROI networks were not investigated in detail because the initial results from the disconnectivity graphs did not indicate any promising results. It likely these networks would result, like the DMN, to have no significant potential biomarker states. However, a full investigation in the future may be warranted as the more detailed examinations of the SAL, FPN, and ATN did find potential biomarkers after the t-test performed on the states of the disconnectivity graph did not.

5. CHALLENGES AND FUTURE STUDY

There were many challenges encountered in this project. One particularly difficult part was learning to use SPM and REX properly to process the fMRI data. The documentation is sparse and quite technical. However, once the proper procedure was understood and the proper files installed correctly, the analysis was fairly straightforward. MATLAB scripts were required to process ROI output files from REX, but not difficult and once the proper algorithm and formatting was written became mostly a data management exercise

Another difficulty was formatting the given (fMRI) data into proper form for input into Energy Landscape program. It was originally unclear how the data was binarized until a deep dive was taking into the ELAT code in MATLAB. An issue was discovered in how the program was choosing to binarize the data from REX, resulting in rounding every value up to 1 instead of up to 1 and down to 0 (or-1), as intended.

Further issues with the ELAT stalling when processing the large iterations of the algorithms in the MATLAB code required altering the iterations from 5,000,000 to 1,000,000 (see Figure 16) to enable the program to fully process without freezing. It is assumed that this is a result of the limitations of the computer hardware available for this study. A more powerful PC would most likely be able to process it at the default 5,000,000 iterations. The lack of any potential biomarker states in the DMN-R sub-network indicates that dividing the network was not successful. It may have been a more fruitful to re-process the full DMN using a limited iteration algorithm than to divide the network into left and right sides.

While the most promising networks were chosen based on the initial energy landscape discontinuity graphs, a further analysis of all ROI states of the Cingulo-Opercular, Sensorimotor, Subcortical, Visual, and Auditory networks using similar methods may uncover further potential biomarkers. A fuller examination of these networks is left up to future studies.

Perhaps the most challenging difficulty came in interpreting the results in meaningful way and with enough context. Unfortunately, this means the analysis of even the ROI networks that were examined in detail remains incomplete. Researchers who have more expertise in biology may be able to formulate more insightful hypothesis from the data presented and conduct further studies into the potential biomarkers identified. More detailed interpretation is left to future work.

```
function [h,J] = pfunc_02_Inferrer_ML(binarizedData)
% 2016/11/11 by T. Ezaki
% This function infers h and J by maximum likelihood estimation.
% binarizedData: nodeNumber x tmax
[nodeNumber,dataLength] = size(binarizedData);

% tuning parameters
% iterationMax = 5000000;
% permissibleErr = 0.00000001;

% Relaxed tuning parameters for computer performance issues - Jeff Feb 2022
iterationMax = 1000000;
permissibleErr = 0.00000002;

dt = 0.2;

dataMean = mean(binarizedData,2);
dataCorrelation = (binarizedData*binarizedData')/dataLength;

h = zeros(nodeNumber,1);
J = zeros(nodeNumber);

for t=1:iterationMax
    [modelMean, modelCorrelation] = mfunc_ModelMeanCorrelation(h,J);
    dh = dt * (dataMean-modelMean);
    dJ = dt *  (dataCorrelation-modelCorrelation);
    dJ = dJ - diag(diag(dJ));% Jii = 0
    h = h + dh;
    J = J + dJ;
```

Figure 16. The recursion in the Energy Landscape functions had to be lowered in order to analyze the data on the PC hardware used.

6. CONCLUSION

Even with the limited data available, technical challenges with data processing, and incomplete analysis of the results we were still able to identify some promising ROI states which have possibilities to be strong biomarkers for future ADHD diagnosis using fMRI techniques, especially in the SAL and FPN. While the utility of the specific ROI brain states examined in this study as biomarkers may be nebulous, we believe the results significant enough to be worthy of further study, and hopefully studies like this will inspire further examination of brain disorders via energy landscape analysis.

fMRI is a powerful tool for investigation, and perhaps soon diagnosis, of brain function of neuro-atypical populations, such as subjects with ADHD. The data intensive nature of Energy Landscape analysis can be challenging, but with more computational resources and faster processing times energy landscape analysis will become easier use, making conclusive results more possible and lots of opportunity for further study in these areas. The application of Energy Landscape analysis to fMRI data is a rich source of future study.

REFERENCES

[1] Ezaki, T., et al., "Energy landscape analysis of neuroimaging data." Philosophical Transactions of The Royal Society A: Mathematical Physical and Engineering Sciences 375. (2017) 10.1098/rsta.2016.0287

[2] Ezaki, T., Masuda, N., "Energy Landscape Analysis Toolbox Version (3.2)." Github. (2018) https://github.com/tkEzaki/energy-landscape-analysis (accessed 12 January 2022).

[3] Mayo Clinic Staff. "Adult attention-deficit/hyperactivity disorder (ADHD)." Mayo Clinic website, https://www.mayoclinic.org/diseases-conditions/adult-adhd/symptoms-causes/syc-20350878 (accessed 5 May 2021).

[4] NITRC staff. "FCP Classic Data Sharing Samples." Neuroimaging Tools & Resources Collaboratory (NITRC). http://fcon_1000.projects.nitrc.org/fcpClassic/FcpTable.html (accessed 19 April 2021).

[5] Milham, M., "1000 Functional Connectomes Later: Where We Are and Where We Are Going." Neuroimaging Tools & Resources Collaboratory (NITRC). Second Biennial Resting-State Conference, Milwaukee, WI, Sept. 18-21

[6] Jahn, A., "fMRI Short Course with FSL." Andy's Brain Book, University of Michigan (2021). andysbrainbook.readthedocs.io/en/latest/fMRI_Short_Course/fMRI_Intro.html (accessed 5 May 2021).

[7] Whitfield-Gabrieli, S., "REX MANUAL." MIT website, http://web.mit.edu/swg/software.htm (2009)

APPENDIX
FULL ENERGY LANDSCAPE ANALYSIS RESULTS

Cingulo-Opercular (CON) Network

ADHD scores

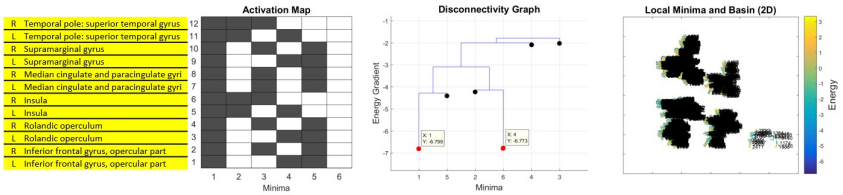

CONTROL scores

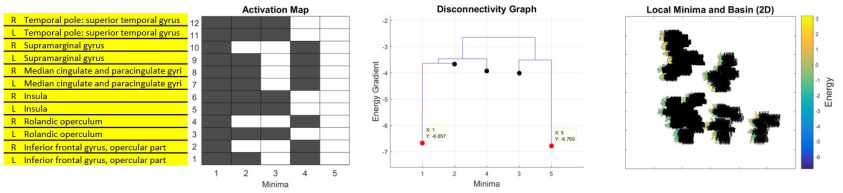

Sensorimotor (SSM) Network

ADHD scores

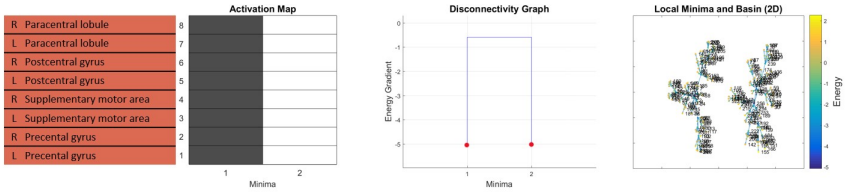

CONTROL scores

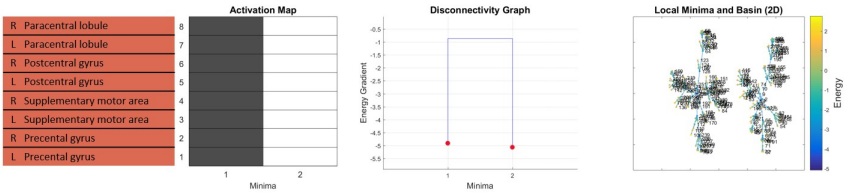

Subcortical (SUB) Network

ADHD scores

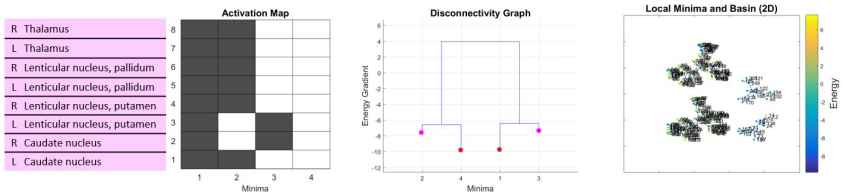

CONTROL scores

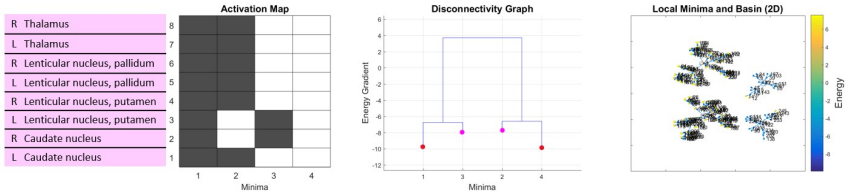

Auditory (AUD) Network

ADHD scores

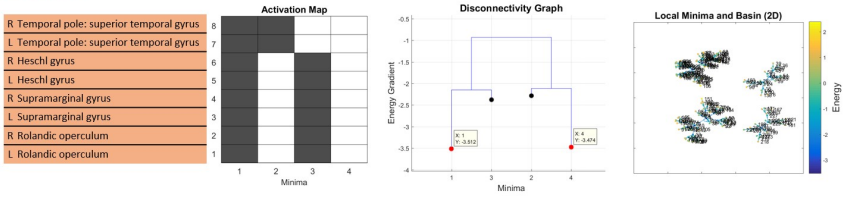

CONTROL scores

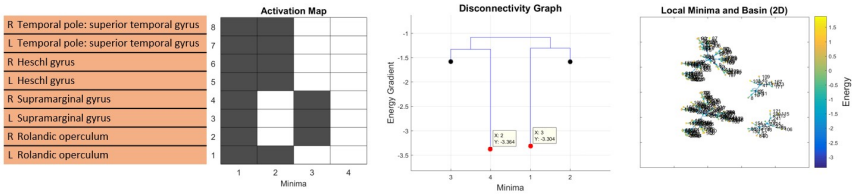

Salience (SAL) Network

ADHD scores

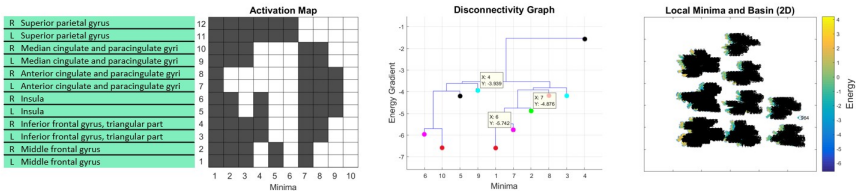

CONTROL scores

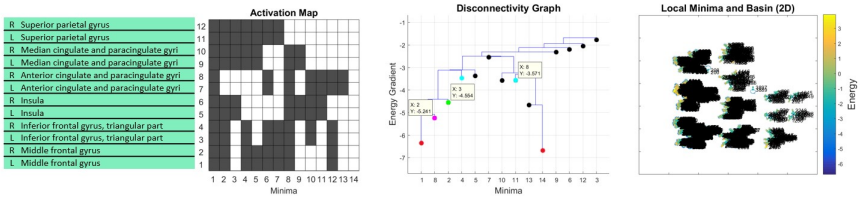

Frontoparietal (FPN) Network

ADHD scores

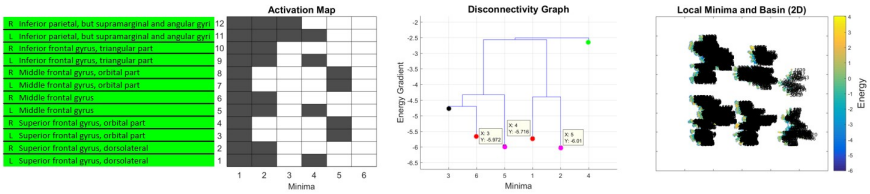

CONTROL scores

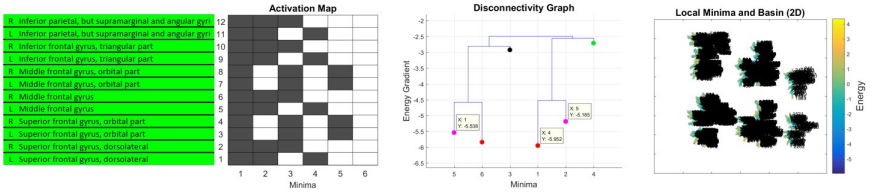

Attention (ATN) Network

ADHD scores

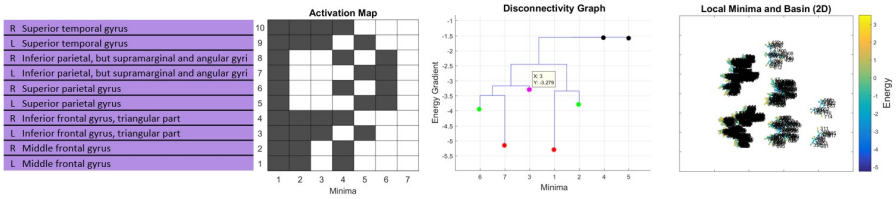

CONTROL scores

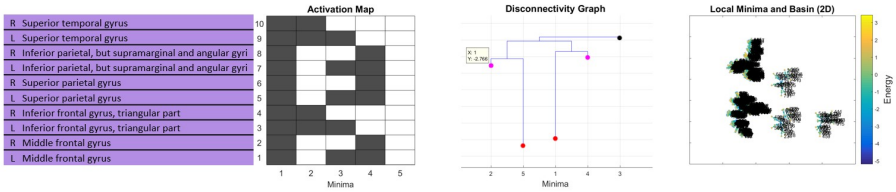

Visual (VIS - Left) Network

ADHD scores

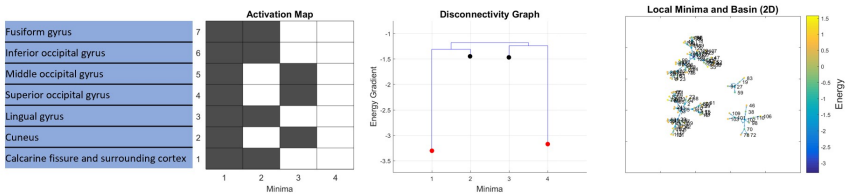

CONTROL scores

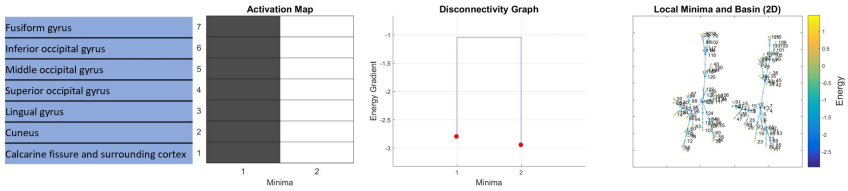

Visual (VIS - Right) Network

ADHD scores

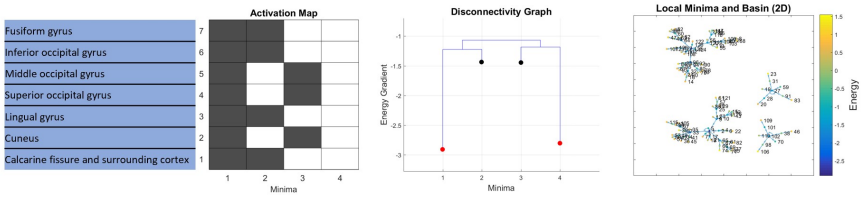

CONTROL scores

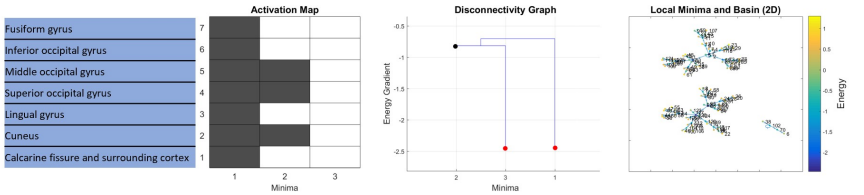

Default-mode (DMN-Left side) Network

ADHD scores

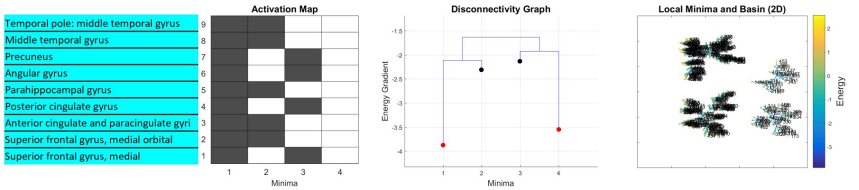

CONTROL scores

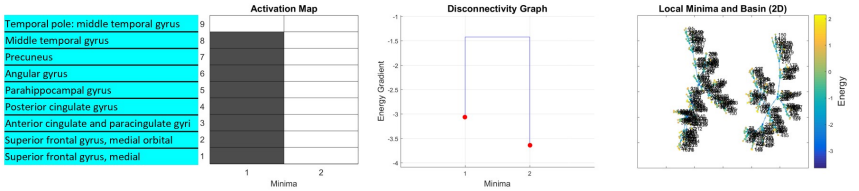

Default-mode (DMN-Right side) Network

ADHD scores

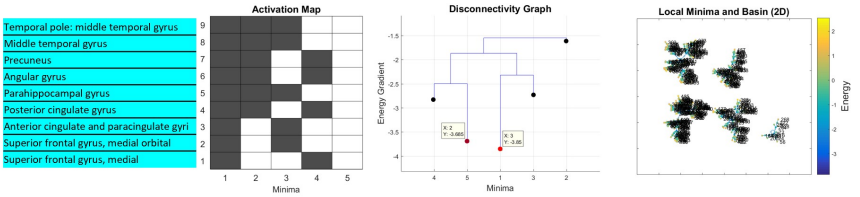

CONTROL scores